Journal of Applied Electrochemistry **34**: 517–524, 2004.

Electrochemical study of Co-based alloys in simulated physiological solution

A. KOCIJAN[1,*], I. MILOŠEV[1], D.K. MERL[1] and B. PIHLAR[2]
[1]*Jožef Stefan Institute, Jamova 39, 1000 Ljubljana, Slovenia*
[2]*Faculty of Chemistry and Chemical Technology, Aškerčeva 5, 1000 Ljubljana, Slovenia*
*(*author for correspondence, fax: +386 1 4773 811, e-mail: aleksandra.kocijan@ijs.si)*

Received 6 July 2003; accepted in revised form 24 November 2003

Key words: Co-based alloys, complexing agents, corrosion, cyclic voltammetry, physiological solution

Abstract

The aim of the present work was to provide a better understanding of the biocompatibility of Co-based alloys in the physiological environment. Co-based alloys are widely used in orthopaedics for the manufacture of prosthetic devices. Two alloys, Co–Cr–Mo and Co–Ni–Cr–Mo, and their individual metal components were studied in simulated physiological solution at 37 °C, with and without the addition of two complexing agents, EDTA and citrate, in the concentration range from 0.1 to 50 mM. The processes were studied using electrochemical techniques: cyclic voltammetry, anodic potentiodynamic measurements, linear polarization and electrochemical impedance spectroscopy. The results are discussed in the context of the dependence of the passivation behaviour of the two alloys on their composition. Both alloys are shown to passivate very well in simulated physiological solution. The effect of complexing agents is more evident on Co–Ni–Cr–Mo than on Co–Cr–Mo alloy. This appears to be related to the presence of Ni.

1. Introduction

Surgical grade Co-based alloys are widely used for the manufacture of prosthetic devices. Their extensive use is based on their superior resistance to corrosion and biodegradation and to their good mechanical properties, including high ultimate tensile and fatigue strength combined with sufficient elongation at fracture [1]. The implanted metal is submitted to simultaneous effects of mechanical and chemical interactions [2]. In the course of time the alloy itself and its corrosion products can react directly with the surrounding tissues, be transported by the bloodstream to distant organs or be partially eliminated by body fluids. On long-term accumulation of metal corrosion products in internal organs such as liver and kidney, the tolerance level may be exceeded, leading to conditions under which certain diseases may be provoked [3].

The performance of Co-based alloys has encouraged several authors to study their mechanical properties, corrosion behaviour and their degree of tolerance by tissues under conditions similar to physiological [1–6]. Codaro and coworkers [2] studied the corrosion behaviour of Co–Cr–Mo alloy in 0.15 M NaCl solution at 25 °C using electrochemical impedance spectroscopy and X-ray diffraction tests. The mechanism of passivation involves the spontaneous formation of a film which protects the metal surface. Lucas and coworkers [1] evaluated the susceptibility *in vitro* and *in vivo* of the Co–Cr–Mo alloy to pitting corrosion under static conditions. *In vitro* polarization results showed that passivation treatments are beneficial, lowering the corrosion rate and shifting the breakdown potentials towards more positive values. Silva and coworkers [4] investigated the effect of laser treatment on the corrosion behaviour of cobalt alloys, based on the assumption that the elimination of carbide precipitates and voids could improve both corrosion and mechanical properties of the material. Laser treatment was not detrimental to Co alloys in terms of corrosion resistance, but modified the amount of Cr and oxygen incorporated in the surface film. Devine and Wulff [5] compared the crevice corrosion behaviour of Co–Cr-based surgical implant alloys in deaerated isotonic salt solution and in 10% HCl + 1% $FeCl_3$ solution. Hot isostatic pressing of cast implants, solubilizing heat-treatment and hot working improved the strength and corrosion resistance of these alloys. Özçelik and coworkers [6] studied the corrosion behaviour of Co–Cr–Mo orthopaedic implants in Hank's solution at pH 4.7 and 9. Pitting potentials of the alloy increased at higher pH and corrosion resistance decreased.

The natural, aggressive environment of the human body is difficult to simulate. In the present work Co–Cr–Mo and Co–Ni–Cr–Mo alloys and their individual metal components (Co, Cr, Ni, and Mo) are studied in simulated physiological solution (SPS), with and without the addition of complexing agents EDTA and citrate. The latter simulated the influence of biomolecules, which *in vivo* can act as complexing

agents for metal ions. The study is conducted using electrochemical techniques of cyclic voltammetry, anodic potentiodynamic measurements and linear polarization, and electrochemical impedance spectroscopy (EIS).

2. Experimental details

The pure metal components Co, Cr, Ni and Mo (all 99.9 wt %) were obtained from Metalle und Materialien GmbH, Nürnberg, Germany. Alloys were cut from original prostheses (Protek, Sulzer, Bern, Switzerland). Alloy composition was confirmed by energy dispersive X-ray analysis (EDA) as follows: 27.9 at % Cr, 3.4 at % Mo, 1.6 at % Si, 0.7 at % Fe and the remainder Co, denoted as Co–Cr–Mo alloy (ASTM F75, 1982) [7], and 23 at % Cr, 36 at % Ni, 6.1 at % Mo, 1 at % Ti, 0.5 at % Fe and the remainder Co, denoted as Co–Ni–Cr–Mo alloy (ASTM F562, 1984) [7].

Experiments were carried out at 37 °C in Hank's solution, a simulated physiological solution (SPS), which contained 8 g L^{-1} NaCl, 0.40 g L^{-1} KCl, 0.35 g L^{-1} $NaHCO_3$, 0.25 g L^{-1} $NaH_2PO_4 \cdot 2\,H_2O$, 0.06 g L^{-1} $Na_2HPO_4 \cdot 2\,H_2O$, 0.19 g L^{-1} $CaCl_2 \cdot 2\,H_2O$, 0.41 g L^{-1} $MgCl_2 \cdot 6\,H_2O$, 0.06 g L^{-1} $MgSO_4 \cdot 7\,H_2O$ and 1 g L^{-1} glucose. Complexing agents, EDTA (ethylenediaminetetraacetic acid disodium salt dihydrate) and citrate (tri-sodium citrate dihydrate), were added to concentrations of 0.1, 5 and 50 mM. In all cases pH values were adjusted to physiological pH 7.8. All chemicals were from Merck, Darmstadt, Germany.

The test specimens were cut into discs of 15 mm diameter. The specimens were abraded with SiC emery paper down to a 1000-grit and rinsed with distilled water. The specimens were then embedded in a Teflon PAR holder and employed as a working electrode. The reference electrode was a saturated calomel electrode (SCE, 0.242 V vs SHE) and the counter electrode was a high purity graphite rod.

Cyclic voltammetry, potentiodynamic and linear polarization measurements were recorded using an EG&G PAR PC-controlled potentiostat/galvanostat (model 263) with M252 and Softcorr computer programs. In the case of potentiodynamic measurements and linear polarization the specimens were immersed in the solution 1 h prior to the measurement in order to stabilize the surface at the open-circuit potential. Potentiodynamic curves were recorded starting 250 mV more negative than the open-circuit potential. The potential was then increased, using a scan rate of 1 mV s^{-1}, until the transpassive region was reached. Linear polarization curves were recorded ±10 mV around the open-circuit potential using a scan rate of 0.1 mV s^{-1}. In cyclic voltammetry a scan rate of 20 mV s^{-1} was used unless stated otherwise.

Electrochemical impedance spectroscopy (EIS) measurements were made using a frequency response analyser (Solartron 1250) combined with a potentiostat/galvanostat (Solarton 1286) and ZPlot computer program. Impedance spectra were measured for both alloys. The working electrode (Co–Cr–Mo or Co–Ni–Cr–Mo alloy) was polarized at potentials of −0.7, −0.3, 0.1, 0.6 and 0.8 V vs SCE in correlation with the cyclic voltammograms. Quasi steady-state current was usually attained within 15 min. The potential was then jumped to the value of interest and the impedance spectra collected within the frequency range of 10 kHz to 1 mHz with an excitation signal amplitude of 10 mV.

3. Results

3.1. *Polarization measurements*

Corrosion current density (i_{corr}) and potential at zero current ($E(I = 0)$) values for Co–Ni–Cr–Mo and Co–Cr–Mo alloys and Co, Cr, Ni and Mo metals in SPS containing different concentrations of citrate and EDTA are presented in Figure 1. The calculations are performed from linear polarization measurements using the equation:

$$R_p = \frac{\beta_a \beta_c}{2.3\, I_{corr}(\beta_a + \beta_c)}$$

Polarization resistance, R_p, is evaluated from linear polarization curves by applying a linear least-squares fit of the data around ±10 mV E_{corr}. The corrosion current, I_{corr}, is calculated from R_p, the least-squares slope, and the Tafel constants, β_a and β_c, of

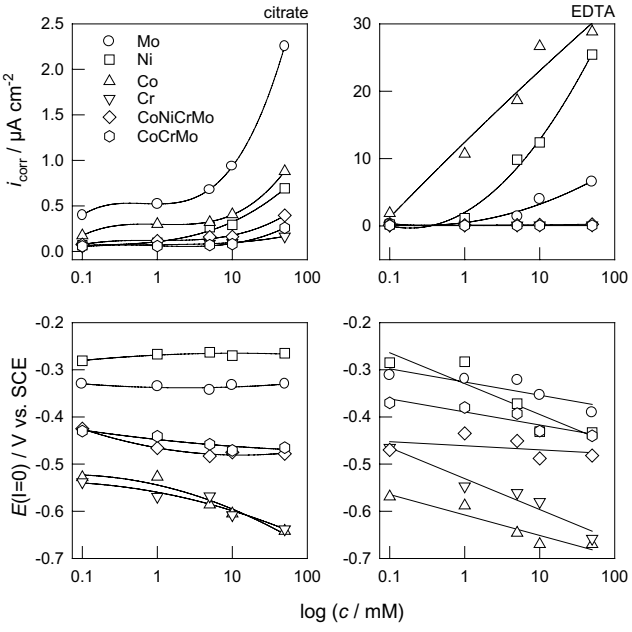

Fig. 1. Values of exchange current density and corrosion potential as a function of logarithm of concentration of EDTA and citrate.

100 mV decade^{-1}. The value of $E(I = 0)$ is calculated from the least-squares intercept.

The values of $E(I = 0)$ shift to more negative values in the presence of complexing agents. In EDTA, $E(I = 0)$ shifts rapidly to more negative values for Co, Cr and Ni, but not for the alloys and Mo. In citrate, the shift is largest for Co and Cr but almost negligible for the alloys, Ni and Mo. Corrosion current density, on the other hand, increases with increasing concentration of complexing agents. In citrate, the increase is greatest for Mo, where the value of i_{corr} increases from approximately 0.5 to 2.5 μA cm^{-2}. In EDTA containing solution, corrosion current density increases much more than in citrate. The largest increase is observed for Co and Ni, where the values are approximately 100-fold greater than those in citrate. Corrosion current density values of alloys are not changed significantly by the addition of complexing agent.

Figure 2 shows anodic potentiodynamic curves for Co–Ni–Cr–Mo and Co–Cr–Mo alloys and for metal components in SPS, with and without the addition of 50 mM citrate. After 1 h stabilization at the open-circuit potential, corrosion potential (E_{corr}) for Co in SPS is −0.52 V, for Mo −0.32 V, for Ni −0.28 V, for Cr −0.58 V, for Co–Ni–Cr–Mo alloy −0.50 V and for Co–Cr–Mo alloy −0.55 V. Following the Tafel region, both alloys and all metals except Mo exhibit passive behaviour. The extent of the passive range increases from Co, to Ni, to Cr and both alloys. The passive range is limited by the breakdown potential (E_b), which is defined as the potential at which the current density in the passive range starts to increase abruptly. The breakdown potential for Co in SPS is −0.25 V, for Mo 0 V and for Ni 0.12 V, whereas chromium and both alloys exhibit similar values of about 0.45 V. In the presence of citrate, Co and Mo show no tendency to passivate. Ni and both alloys passivate in SPS containing citrate, however, the breakdown potentials are moved by approximately 0.1 V to more negative values. The passivation behaviour of Cr remains apparently unaffected by the addition of citrate.

EDTA induces a somewhat stronger effect than citrate on the corrosion resistance of the alloys and their metal components (Figure 1).

3.2. *Cyclic voltammetry*

Co–Ni–Cr–Mo and Co–Cr–Mo alloys and individual metal components (Co, Cr, Ni and Mo) were further studied using cyclic voltammetry.

The influence of potential scan rate on the behaviour of Co–Cr–Mo alloy in SPS is presented in Figure 3(a). There is no anodic peak and the passive range extends from −0.9 to 0.4 V. The current density of peak B increases with increasing scan rate. For Co–Ni–Cr–Mo alloy (Figure 3(b)) the peak A at −0.3 V is observed in the anodic cycle. Its current density increases and the potential shifts in the positive direction with increasing scan rate. The peak B at 0.2 V in the cathodic cycle is observed for scan rates of 50 and 100 mV s^{-1} for Co–Cr–Mo and Co–Ni–Cr–Mo alloys.

The influence of scan rate on cyclic voltammograms recorded for alloys in SPS containing 50 mM of citrate is shown in Figure 4. For Co–Cr–Mo alloy the results are

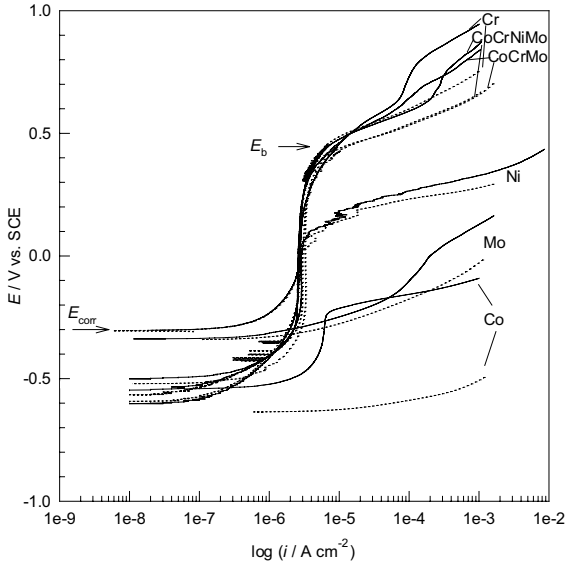

Fig. 2. Anodic polarization curves recorded for Co–Ni–Cr–Mo, Co–Cr–Mo alloy and their individual metal components in SPS with (—) and without (···) the addition of 50 mM citrate. Scan rate 1 mV s^{-1}.

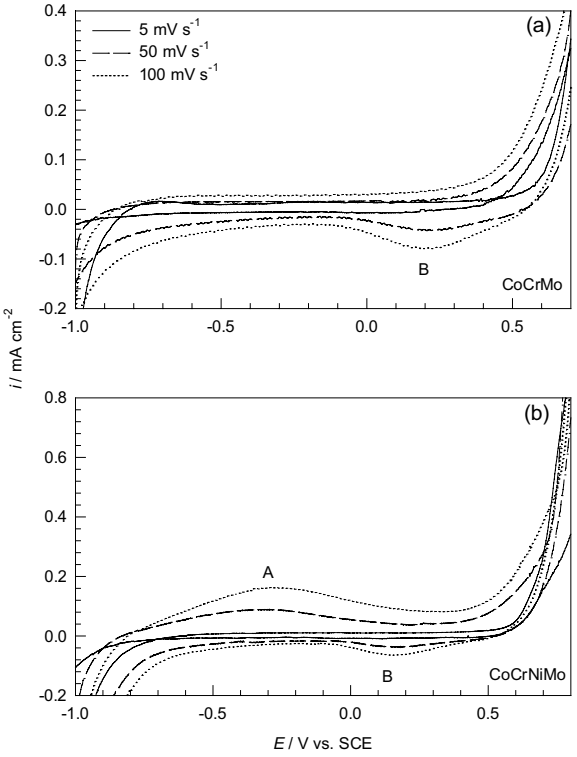

Fig. 3. Cyclic voltammograms recorded for (a) Co–Cr–Mo and (b) Co–Ni–Cr–Mo alloy with increasing potential scan rate, dE/dt: 5, 50 and 100 mV s^{-1} in SPS.

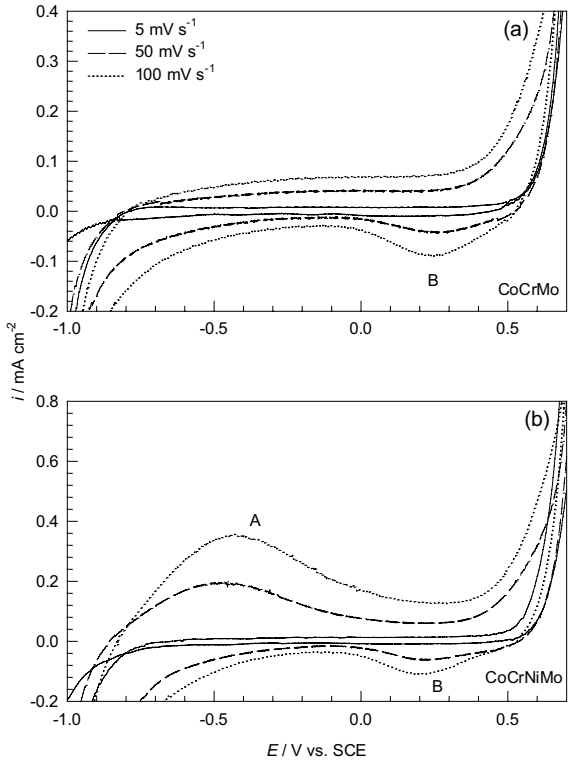

Fig. 4. Cyclic voltammograms recorded for (a) Co–Cr–Mo and (b) Co–Ni–Cr–Mo alloy with increasing potential scan rate, dE/dt: 5, 50 and 100 mV s^{-1} in SPS containing 50 mM of citrate.

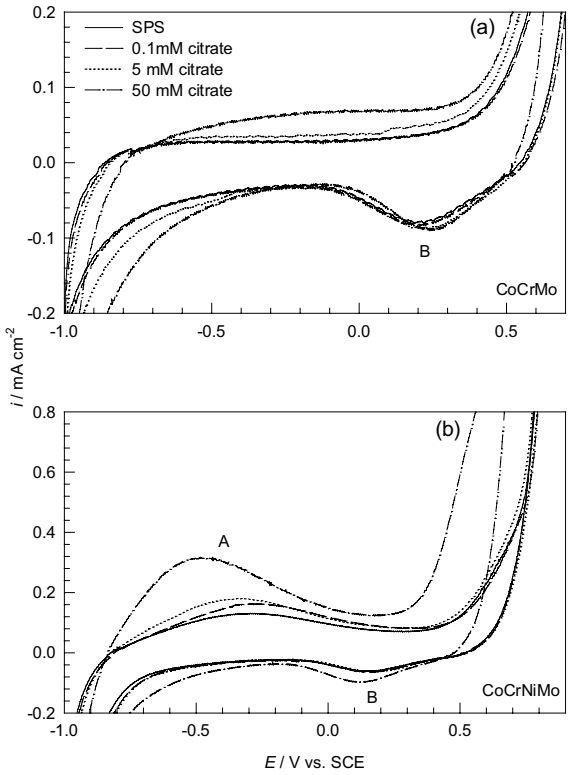

Fig. 5. Cyclic voltammograms recorded for (a) Co–Cr–Mo and (b) Co–Ni–Cr–Mo alloy in SPS containing various concentrations of citrate: 0, 0.1, 5, 50 mM. Scan rate 100 mV s^{-1}.

similar to those obtained in pure SPS (Figure 3(a)), with a single peak B in the cathodic cycle. For Co–Ni–Cr–Mo alloy peak A in the anodic cycle and peak B in the cathodic cycle are observed. Compared to SPS, the current density of peak A increases and its potential shifts appreciably towards more positive values, that is, from −0.6 to −0.4 V. The potential of peak B shifts only slightly.

Figure 5 shows the influence of different concentrations of citrate on cyclic voltammograms recorded for the alloys at a scan rate of 100 mV s^{-1}. The current density of Co–Cr–Mo alloy in the passive range is not significantly affected by increasing citrate concentrations (Figure 5(a)). The position and current density of peak B remain practically identical for all citrate concentrations. On the other hand, the behaviour of Co–Ni–Cr–Mo alloy is strongly affected by the addition of citrate (Figure 5(b)). The position of peak A shifts linearly from −0.25 V in SPS to −0.5 V in 50 mM citrate, and its current density increases with citrate concentration. The potential in the beginning of the transpassive oxidation shifts towards more negative values with increasing citrate concentration. In the cathodic cycle the potential of peak B at 0.2 V shifts towards somewhat more negative values and its current density increases only slightly with citrate. In EDTA containing solutions similar results were obtained.

Cyclic voltammograms for individual metal components were recorded at a scan rate of 100 mV s^{-1} in SPS, containing 50 mM of EDTA and 50 mM of citrate (Figure 6).

Cobalt passivates in SPS in the range from −0.75 to −0.1 V (Figure 6(a)), due to the formation of CoO, in accordance with reaction 1 (Table 1). Cobalt forms two different passive layers, depending on the potential [8–10]. The primary passive layer consists of CoO and is formed at low potentials. At high potentials a secondary passive layer is formed consisting of Co(II)/Co(III) mixed oxides, during the transpassive oxidation at $E > 0.1$ V (Reaction 2, Table 1) [8–11]. The peak at −0.9 V in the reverse cycle corresponds to the reduction of Co(II) to Co (Reaction 1, Table 1) [11]. With the addition of EDTA the passive range is interrupted by an increase in current density at −0.6 V. At higher concentrations of EDTA the transpassive peak appears at −0.2 V, presumably related to the formation of Co(III) (insert in Figure 6(a), Reaction 2, Table 1) [11, 12]. The main cathodic peak at −0.95 V, related to the reduction of CoO to Co, increases (Reaction 1, Table 1) [11]. In SPS containing citrate, the cathodic peak is shifted to −0.85 V and its current density increases further.

Molybdenum passivates in SPS in the range from −0.9 to −0.1 V, in accordance with the formation of MoO_2 (Reaction 3, Table 1, Figure 6(b). Passive current density starts to increase abruptly at 0 V due to the transpassive oxidation of Mo(IV) to Mo(VI) (Reaction 4, Table 1), where molybdate and/or heptamolybdate species were identified [13]. In SPS containing EDTA

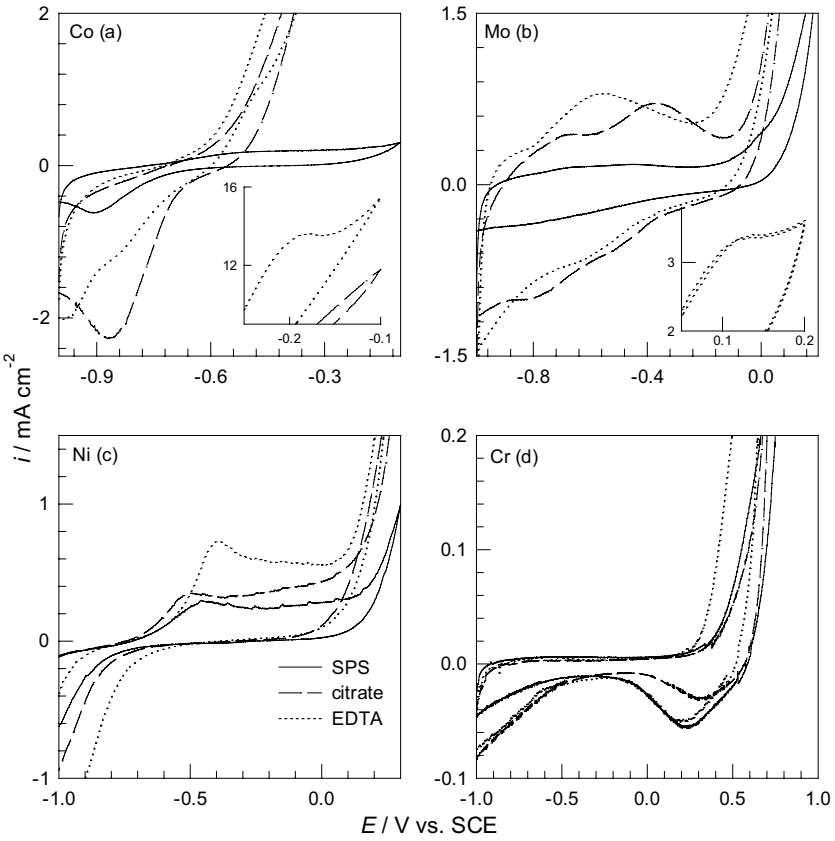

Fig. 6. Cyclic voltammograms recorded for individual metals (a) cobalt, (b) molybdenum, (c) nickel and (d) chromium in SPS and with the addition of 50 mM citrate or EDTA. Scan rate 100 mV s^{-1}.

and citrate the current density increases over the whole potential range and two additional peaks appear, probably related to the formation of species of higher oxidation states. The potential where transpassive oxidation begins is shifted to a more negative value (i.e., −0.2 V).

The cyclic voltammogram for Ni in SPS shows an anodic peak at −0.5 V, related to the formation of NiO (Reaction 5, Table 1, Figure 6(c)) [14] causing the establishment of the passive region extending up to 0.2 V. At more positive potentials transpassive nickel dissolution and oxygen evolution take place (Reaction 6, Table 1) [14]. In the presence of complexing agents the current density of the anodic peak increases, the peak potential shifts slightly and the passive region narrows (Figure 6(c)).

Cr passivates readily in SPS due to the spontaneous formation of Cr_2O_3 (Reaction 7, Table 1, Figure 6(d)) [15, 16]. The wide region of passivity extends from −0.9 to 0.6 V. At $E > 0.5$ V Cr undergoes transpassive oxidation accompanied by the formation of Cr(VI) species (Reaction 8, Table 1) [16]. Some of the Cr(VI) species remains incorporated in the passive film and is reduced in a solid state reduction process in the region of the peak at 0.2 V [16, 17]. The addition of complexing agents does not appreciably affect the shape of the curve of chromium. EDTA and citrate form very strong complexes with Cr^{3+} ions [12], but due to the very slow dissolution of the strongly protective Cr_2O_3 layer, the amount of Cr(III) species available for complexing is small [18].

Table 1. Possible reactions occurring at particular regions in cyclic voltammograms of Co–Ni–Cr–Mo, Co–Cr–Mo alloy and their individual metal components [24]

No.	Reaction	Equilibrium potential
1	$Co + H_2O \leftrightarrow CoO + 2\,H^+ + 2\,e^-$	$E_o = 0.095 - 0.059$ pH
2	$2\,Co^{2+} + 3\,H_2O \leftrightarrow Co_2O_3 + 6\,H^+ + 2\,e^-$	$E_o = 1.746 - 0.177$ pH $- 0.059 \log [Co^{2+}]$
3	$Mo + 2\,H_2O \leftrightarrow MoO_2 + 4\,H^+ + 2\,e^-$	$E_o = -0.072 - 0.059$ pH
4	$MoO_2 + 2\,H_2O \leftrightarrow MoO_4^{2-} + 4\,H^+ + 2\,e^-$	$E_o = 0.606 - 0.118$ pH $+ 0.029 \log [MoO_4^{2)}]$
5	$Ni + H_2O \leftrightarrow NiO + 2\,H^+ + 2\,e^-$	$E_o = 0.116 - 0.059$ pH
6	$Ni^{2+} + 2\,H_2O \leftrightarrow NiO_2 + 4\,H^+ + 4\,e^-$	$E_o = 1.593 - 0.118$ pH $- 0.029 \log [Ni^{2+}]$
7	$2\,Cr + 3\,H_2O \leftrightarrow Cr_2O_3 + 6\,H^+ + 6\,e^-$	$E_o = -0.654 - 0.059$ pH
8	$Cr_2O_3 + 5\,H_2O \leftrightarrow 2\,CrO_4^{2-} + 10\,H^+ + 6\,e^-$	$E_o = 1.311 - 0.098$ pH $+ 0.019 \log [CrO4^{2)}]$

Table 2. Values of fitting parameters for Co–Cr–Mo and Co–Ni–Cr–Mo alloy in SPS with and without the addition of 50 mM citrate and EDTA at different polarization potentials

Alloy	Solution	E /V	R_1 /Ω cm^{-2}	$Q_1 \times 10^{-5}$	n_1	R_2 /Ω cm^{-2}	$Q_2 \times 10^{-5}$	n_2
Co–Cr–Mo	SPS	−0.7	7004	6.60	0.82	71 998	32	0.57
		−0.3	770 000	1.56	0.95			
		0.1	570 000	1.83	0.89			
		0.6	1834	30	0.83			
		0.8	214.8	31	0.80			
	citrate	−0.7	5230	6.80	0.86	64 240	15.1	0.52
		−0.3	530 000	2.60	0.96			
		0.1	250 000	1.95	0.84			
		0.6	391	39	0.80			
		0.8	75.3	44	0.83			
	EDTA	−0.7	2860	8.40	0.87	55 350	26.5	0.52
		−0.3	460 000	2.80	0.98			
		0.1	180 000	2.90	0.89			
		0.6	320	52	0.80			
		0.8	32.1	58	0.80			
Co–Ni–Cr–Mo	SPS	−0.7	1660	6.80	0.84	72 327	40	0.57
		−0.3	38 405	1.46	0.89			
		0.1	870 000	29	0.90			
		0.6	411	47	0.82			
		0.8	173.6	6.90	0.82			
	citrate	−0.7	1441	7.70	0.88	48 307	62	0.53
		−0.3	7316	5.3	0.87			
		0.1	820 000	1.34	0.90			
		0.6	265	58	0.81			
		0.8	57.8	67	0.85			
	EDTA	−0.7	719	8.85	0.88	11 640	150	0.53
		−0.3	3977	6.60	0.90			
		0.1	680 000	1.79	0.89			
		0.6	173	53	0.81			
		0.8	27.8	71	0.87			

3.3. *Impedance measurements*

To estimate polarization resistance (R_p) in impedance measurements, a fitting procedure using equivalent circuits consisting of resistance and capacitance elements, was used. For our purpose simple RQ elements in series with the R_s were used. In the cases where two semicircles were observed, 2 RQ elements in series with R_s were used. The high frequency intercept R_s is ascribed to the electrolyte bulk resistance and is seen clearly only in anodic polarization, due to the smaller scale. At lower frequencies, a main arc appears, due to interfacial processes at the phase metal–electrolyte. Interception of this arc with the real axis is ascribed to the polarization resistance ($R_p = R_1$ or $R_p = R_1 + R_2$). Element Q (constant phase element) is defined as [19]:

$$Q = Z_{cpe} = C^{-1}(j\,\omega)^{-n}$$

For $n = 1$, the Q element reduces to a capacitor with capacitance C and, for $n = O$, to a simple resistor. $n = 0.5$ shows diffusion characteristic of the detected processes. $j = (-1)^{1/2}$; ω is the angular frequency.

Impedance spectra were measured at −0.7, −0.3, 0.1, 0.6 and 0.8 V, in accordance with the polarization curves in Figure 2. Evidently, the shape as well as the order of magnitude of the impedance response, depends markedly on the applied d.c. potential. Values of fitted parameters for both alloys at different potentials in selected environments are presented in Table 2.

At very negative potentials (i.e., −0.7 V), where cathodic current is still obtained, two arcs appear in the impedance spectra (Figure 7(a)). The high frequency arc can be ascribed to the cathodic reaction. R_p values were of the order of 1000 Ω cm^{-2}. The origin of the lower frequency arc is probably related to the diffusion process connected with the reduction reaction. This is supported by the value of n_2, which is close to 0.5 (Table 2) and is characteristic of a diffusion process [19].

At −0.3 and 0.1 V, the impedance response consists of a single arc (Figure 7(b)). Their R_p reached the order of 10^5 Ω cm^{-2}. Such high R_p values show that the passive layer formed on the interface of the alloy is relatively stable (Figure 7(b)), as confirmed by polarization measurements (Figure 2).

At more positive anodic potentials (i.e., 0.6 and 0.8 V), the impedance response consists of a high frequency intercept with the x-axis and an arc with loops at lower frequency (Figure 7(c)), which are characteristic for the reaction of oxidation [20]. R_p values decrease almost fourfold. These data are consistent with the increase in current density at potentials more positive than 0.4 V (Figure 2).

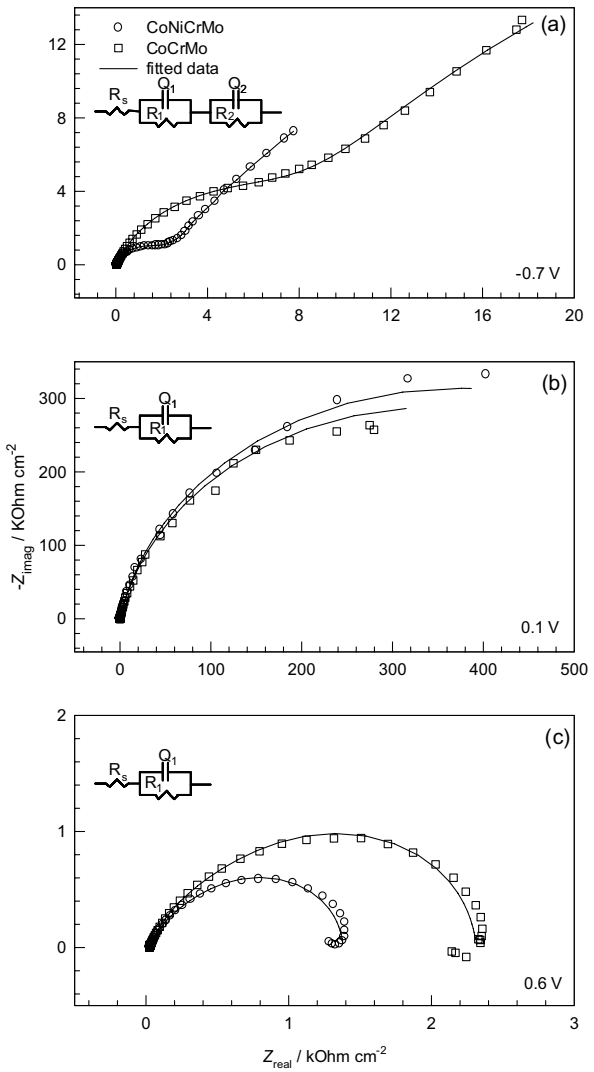

Fig. 7. Nyquist plot recorded for Co–Ni–Cr–Mo and Co–Cr–Mo alloy at (a) −0.7 V, (b) 0.1 V and (c) 0.6 V vs SCE in SPS. Inserts: equivalent circuit models.

4. Discussion

Electrochemical data show that both Co-based alloys passivate very well in simulated physiological solution. Their electrochemical characteristics are similar to those of chromium metal (Figures 3 and 6(d)). It is then reasonable to assume that Cr-oxide would be the major constituent of the passive film formed on these alloys. Indeed, X-ray photoelectron spectroscopy measurements [21] and literature data confirm this hypothesis [22, 23]. The content of chromium oxide in the passive layer formed on Co–Cr–Mo and Co–Ni–Cr–Mo alloy is twice as much as in the bulk alloy. In the case of Co–Cr–Mo alloy, the second major constituent of the passive layer is CoO, which is, however, depleted threefold compared to the content in the bulk. The content of molybdenum oxide is larger in the passive layer than in the bulk alloy [21]. Li et al. obtained similar results when studying the Co–Cr–Mo alloy in biosimulating solutions using surface-enhanced Raman spectroscopy [23]. Cyclic voltamograms of Co–Ni–Cr–Mo alloy differ from those recorded for Co–Cr–Mo alloy by the presence of the peak A (Figures 3–5). Comparing the cyclic voltammograms of individual metal components and the two alloys, it is seen that the main contributor to peak A of Co–Ni–Cr–Mo alloy is the oxidation of nickel. XPS measurements confirm that, in Co–Ni–Cr–Mo alloy, nickel oxide becomes the second major constituent of the passive layer [21]. Cobalt oxide is also identified in the layer but its content is much lower than in the passive layer formed on Co–Cr–Mo alloy.

Impedance data show that the alloy containing Ni is less corrosion resistant in selected environments than Co–Cr–Mo alloy, as indicated by significantly smaller values of R_p at all potentials investigated (Figure 7). The only exception is the potential of 0.1 V, where R_p values of Co–Cr–Mo alloy are smaller than those of Co–Ni–Cr–Mo alloy. Possible reasons could be the experimental scatter, since the measurement precision was poor at lower frequency due to the high resistance, or that interface processes were taking place on Co–Ni–Cr–Mo alloy, that were reflected in a slightly higher resistance. Both alloys are most stable in SPS.

The complexing agents have a pronounced effect on the individual metal components, Ni, Co and Mo, as shown by the increase in corrosion current density, shift of the corrosion potential towards more negative values (Figure 1) and narrowing of the passive region (Figures 2–6). The extent of this effect is obviously related to the stability constants of the metal complexes formed with either EDTA or citrate [15]. Ni and Co form strong complexes with EDTA, with logarithm of the stability constant (log K_{st}) of 16.3 for Co^{2+} and 18.5 for Ni^{2+} [12]. Due to the formation of the metal complexes the current density is expected to increase. This behaviour is illustrated in Figures 2 and 6. In the case of Co the transpassive region is also affected by the addition of complexing agent. The stability constant of Co(III) with citrate is not known but for EDTA log K_{st} is much higher for Co(III) (log $K_{st} = 41.4$) than for Co(II) (log $K_{st} = 16.2$) complex. Therefore, in the transpassive range, that is, $E > -0.5$ V (Figure 6(a)), Co(III) species formed by the transpassive oxidation (Reaction 2, Table 1) will be further complexed by EDTA due to the large value of log K_{st}. No literature data exist for stability constants for complexes of Mo with EDTA or citrate.

The addition of complexing agents affects the two Co-based alloys differently. Whereas in the passive range, Co–Cr–Mo alloy is not significantly affected by the addition of either EDTA or citrate, Co–Ni–Cr–Mo alloy is susceptible to the influence of both complexing agents (Figures 4 and 5). Since the peak A is mainly related to the oxidation of Ni (and Co) it is reasonable to assume that this effect stems from the complex formation of Ni (and Co). Impedance data (Table 2 and Figure 7) confirm that both alloys are more stable in SPS than in the presence of complexing agents, as evident by the decreased values of R_p (Table 2). Com-

pared to peak A, the effect of complexing agents on the reduction of Cr(VI), that is, peak B, is minor, as evidenced by an insignificant dependence of the height and potential of the peak on increasing concentration of complexing agent.

5. Conclusions

The behaviour of Co–Cr–Mo and Co–Ni–Cr–Mo alloys and their individual metal components was studied in simulated physiological solution by cyclic voltammetry, anodic potentiodynamic measurements, linear polarization and electrochemical impedance spectroscopy, with and without the addition of complexing agents, EDTA and citrate. The major constituent of the passive layer formed on both alloys is chromium(III) oxide. Minor constituents of the passive layer on Co–Cr–Mo alloy are oxides of cobalt, molybdenum, whereas Co–Ni–Cr–Mo alloy additionally contains nickel oxide. Its formation is represented by the anodic peak A, which contributes to the oxidation of Ni. The complexing agents have a profound effect on the individual metal components, Ni, Co and Mo, as shown by the increase in corrosion current density, shift of corrosion potential towards more negative values and narrowing of the passive region. This effect is related to the stability constants of particular metal complexes formed with the complexing agents. The Ni-free alloy is not significantly affected by the addition of the complexing agents, whereas Co–Ni–Cr–Mo alloy is affected by both, citrate and EDTA.

These results prove the influence of complexing agents on the corrosion behaviour of the studied alloys. Further studies including biomolecules, which act as actual complexing agents *in vivo*, would be valuable.

References

1. L.C. Lucas, R.A. Buchanan, J.E. Lemons and C.D. Griffin, *J. Biomed. Mater. Res.* **16** (1982) 799.
2. E.N. Codaro, P. Melnikov, I. Ramires and A.C. Guastaldi, *Russian J. Electrochem.* **36** (2000) 1117.
3. K. Merrit, S.A. Brown and N.A. Sharkey, *J. Biomed. Mater. Res.* **18** (1984) 991.
4. R.A. Silva, M.A. Barbosa, R. Vilar, O. Conde, M.D. Belo and I. Sutherland, *J. Mater. Sci.: Mater. in Med.* **5** (1994) 353.
5. T.M. Devine and J. Wulff, *J. Electrochem. Soc.* **123** (1976) 1433.
6. F. Özçelik, J. Gulen, A. Akdogan and S. Piskin, *Prakt. Metallogr.* **36** (1999) 385.
7. 'Annual Book of ASTM Standards', Vol. 13.01. 'Medicinal Devices' (ASTM, Philadelphia, 1988).
8. K.M. Ismail and W.A. Badawy, *J. Appl. Electrochem.* **30** (2000) 1303.
9. W.A. Badawy, F.M. Al-Kharafi and J.R. Al-Ajmi, *Bull. Electrochem.* **16** (2000) 145.
10. A. Foelske and H.-H. Strehblow, *Surf. Interface Anal.* **29** (2000) 548.
11. N. Sato and T. Ohtsuka, *J. Electrochem. Soc.: Electrochem. Sci. Technol.* **125** (1978) 1735.
12. R.M. Smith and A.E. Martell (Eds), 'Critical Stability Constants', Vol. 3 (Plenum Press, New York London, 1977).
13. K. Wang, Y.-S. Li and P. He, *Electrochim. Acta* **43** (1998) 2459.
14. B. MacDougall, D.F. Mitchell and M.J. Graham, *J. Electrochem. Soc.: Electrochem. Sci. Technol.* **127** (1980) 1248.
15. I. Milošev, *J. Appl. Electrochem.* **32** (2002) 311.
16. M. Moffat and R.M. Latanision, *J. Electrochem. Soc.* **139** (1992) 1869.
17. J.A. Bardwell, G.I. Sproule, B. MacDougall, M.J. Graham, A.J. Davenport and H.S. Isaacs, *J. Electrochem. Soc.* **139** (1992) 371.
18. A. Kocijan, I. Milošev and B. Pihlar, *J. Mater. Sci.: Mater. Med.*, **14** (2003) 69.
19. I.D. Raistrick, J.R. Macdonald and D.R. Francschetti, *in* J.R. Macdonald (Ed.), 'Impedance spectroscopy Emphasizing Solid Materials and Systems' (John Wiley & Sons, New York, 1987), chapter 2.
20. N. Bonanos, B.C.H. Steele, W.B. Johnson, W.L. Worell, D.D. Macdonald and M.C.H. McKurbe, *in* J.R. Macdonald (Ed.), 'Impedance spectroscopy Emphasizing Solid Materials and Systems' (John Wiley & Sons, New York, 1987), chapter 4.
21. A. Kocijan, I. Milošev and B. Pihlar, *J. Mater. Sci.*; *Mater. Med.*, submitted.
22. T. Hanawa, S. Hiromoto and K. Asami, *Appl. Surf. Sci.* **183** (2001) 68.
23. Y.-S. Li, K. Wang, P. He, B.X. Huang and P. Kovacs, *J. Raman Spectrosc.* **30** (1999) 91.
24. M. Pourbaix, 'Atlas of Electrochemical Equilibria in Aquous Solutions' (NACE, Cebelcor, Huston, Brussels, 1974).